Unsteady Turbulent Boundary Layers in Adverse Pressure Gradients

Eugene E. Covert* and Peter F. Lorber†
Massachusetts Institute of Technology, Cambridge, Massachusetts

Several characteristics of an unsteady turbulent boundary layer have been measured on the after part of the upper surface of a NACA 0012 airfoil. Data were taken at a chord Reynolds number of 700,000, at geometric angles of attack of 0 and 10 deg, and over a range of reduced frequencies (based upon the semichord) of 0.5-6.4. Mean and unsteady velocity and Reynolds stress profiles are presented, as is the nonlinear coupling from the unsteady motion into the steady motion. Data are presented showing that for this experiment the periodic unsteady turbulent velocity profile becomes independent of the mean adverse pressure gradient at higher reduced frequencies.

Nomenclature

a = elliptic cylinder minor axis
b = elliptic cylinder major axis
c = airfoil chord
c_f = skin friction coefficient $\tau_w/\frac{1}{2}\rho U_\infty^2$
c_p = pressure coefficient, $(P-P_\infty)/\frac{1}{2}\rho U_\infty^2$
H = boundary-layer shape parameter, δ^*/θ
k = reduced frequency, $\omega c/2U_\infty$
p = pressure
Re_θ = Reynolds number based on momentum thickness $U_e\theta/\nu$
U_e = external velocity
U_∞ = freestream velocity
u = velocity component parallel to surface
U_τ = friction velocity, $\sqrt{\tau_w/\rho}$
v = velocity component normal to surface
x = coordinate parallel to surface
y = coordinate normal to surface
α = airfoil angle of attack
β = pressure gradient, $(\delta^*/\tau_w)(dp/dx)$
Γ = pressure gradient, $(\theta/U_e)(dU_e/dx)(Re_\theta)^{1/4}$
δ^* = displacement thickness, $\int_0^\infty (1-u/U_e)\,dy$
θ = momentum thickness, $\int_0^\infty u/U_e(1-u/U_e)\,dy$
ν = kinematic viscosity
ρ = density
τ_w = shear stress at the surface
ϕ = phase lag
ω = radian frequency
$\bar{(\ )}$ = time average
$\tilde{(\ )}$ = periodic component of zero mean
$\langle\ \rangle$ = ensemble average, $\langle u\rangle = \bar{u}+\tilde{u}$
$(\ )'$ = nonperiodic fluctuating component of zero mean, $u=\langle u\rangle+u'$

Presented as Paper 82-0966 at the AIAA/ASME Third Joint Thermophysics, Fluids, Plasma, and Heat Transfer Conference, St. Louis, Mo., June 7-11, 1982; submitted June 18, 1982; revision received March 9, 1983.

*Professor of Aeronautics and Astronautics, Department of Aeronautics and Astronautics and. Director of Gas Turbine and Plasma Laboratory. Fellow AIAA.

†Research Assistant, Department of Aeronautics and Astronautics. Student Member AIAA.

Introduction

RECENTLY Carr[1] presented a survey of the state-of-the-art of measurements on unsteady turbulent boundary layers. In many of these experiments the metric surface is a flat plate or one wall of the wind tunnel. Unsteadiness is frequently introduced by oscillating vanes or shutters located either upstream or downstream of the test surface. Of all the experiments cited, those of Karlsson,[2] Patel,[3] Kenison,[4] Schachenmann and Rockwell,[5] Simpson et al.,[6] and Cousteix et al.[7] have produced data that are perhaps most closely related to that which will be presented below. Several years ago Telionis[8] reviewed the state of understanding of both separated and attached unsteady boundary layers. He concluded that 1) generally the mean profiles are affected very little by the unsteadiness, 2) the pressure gradient has a strong effect on the fluctuations, and 3) the state-of-the-art of turbulence modeling is inadequate. An example of the latter is calculations that predict an overshoot in unsteady velocity amplitude of 1-2% over that at the edge of the boundary layer, while the data show overshoots of 10 times that value for the same conditions. Telionis concluded something fundamental was missing from the models.

In this paper, we will present additional data that characterizes the unsteady turbulent boundary layer. Our metric surface is the upper surface of a NACA 0012 airfoil that is fixed in a wind tunnel. As described below, the unsteady flow is generated by aerodynamic interference at the trailing edge. We will present data on $\langle u\rangle$, $\langle v\rangle$, $\langle u'^2\rangle$, $\langle v'^2\rangle$, and $\langle u'v'\rangle$ and offer some comments on the processes and their limitations.

Description of Experiment

The experiment we are conducting is somewhat different in conception from those referred to in the introduction. As indicated in the introduction, our metric surface is a NACA 0012 airfoil with a chord length of 50.8 cm. It is located between two vertical sidewalls in the MIT Wright Brothers' Memorial Wind Tunnel. The walls are not quite parallel to the flow; rather, they diverge enough to compensate for the effects of boundary-layer growth.

The airfoil may be rotated about the trailing edge to give a mean geometric angle of attack of between 0 and 15 deg. Just downstream of and below the trailing edge, a two-dimensional elliptic cylinder ($b/a=2.12$) is located, with its axis at either $x/c=1.175$, $y/c=-0.275$ or $x/c=1.12$, $y/c=-0.19$. The elliptic cylinder is rotated at 0-3000 rpm through a belt driven by an adjustable speed electric motor. This provides an unsteady perturbation to the flow about the

Table 1 Summary of experimental conditions[a]

k	α, deg	x/c	$\bar{\Gamma}$	$\bar{\theta}/c$	$\bar{H}$	$\overline{Re}_\theta$	$(x/q)\ d\bar{p}/dx$[d]	$(x/q)\ d\bar{P}/dx$	$\bar{U}_e/\bar{U}_e$
0.5	0[b]	0.69	−0.0025	0.0016	1.80	1160	0.381	0.0483	0.021
1.0			−0.0019	0.0016	1.71	1170	0.281	0.0593	0.022
1.5			−0.0032	0.0017	1.74	1340	0.422	0.0575	0.014
2.0			−0.0023	0.0016	1.75	1230	0.334	0.0299	0.0057
3.9			−0.0024	0.0018	1.74	1410	0.297	0.0198	0.0034
6.4			−0.0021	0.0019	1.74	1430	0.255	0.0375	0.0038
0.5	0[b]	0.94	−0.0144	0.0025	1.64	1570	1.71	0.273	0.031
1.0			−0.0151	0.0026	1.71	1670	1.68	0.402	0.038
2.0			−0.0138	0.0025	1.61	1670	1.62	0.203	0.013
6.4			−0.0101	0.0025	1.61	1780	1.19	0.224	0.0078
0.5	10[b]	0.94	−0.0408	0.0090	2.38	5950	0.969	0.173	0.020
1.0			−0.0358	0.0088	2.50	5600	0.891	0.228	0.033
2.0			−0.0401	0.0091	2.18	5980	0.951	0.088	0.0076
3.9			−0.0406	0.0093	2.04	6120	0.947	0.089	0.0048
6.4			−0.0430	0.0095	2.00	6390	0.958	0.109	0.0062
0.5	10[c]	0.94	−0.0297	0.0093	2.56	6390	0.672	0.238	0.040
1.0			−0.0322	0.0094	2.53	6230	0.725	0.262	0.047
2.0			−0.0297	0.0092	2.44	6160	0.689	0.153	0.016
3.9			−0.0306	0.0087	2.22	6420	0.743	0.135	0.0088
6.4			−0.0304	0.0083	2.11	6400	0.769	0.166	0.0079

[a] Freestream velocity is 20 mps, chord Reynolds number $= 6.8 \times 10^5$. [b] Cylinder axis at $x/c = 1.18$, $y/c = -0.28$. [c] Cylinder axis at $x/c = 1.2$, $y/c = -0.19$. [d] The importance of this parameter follows from the discussion in Ref. 12.

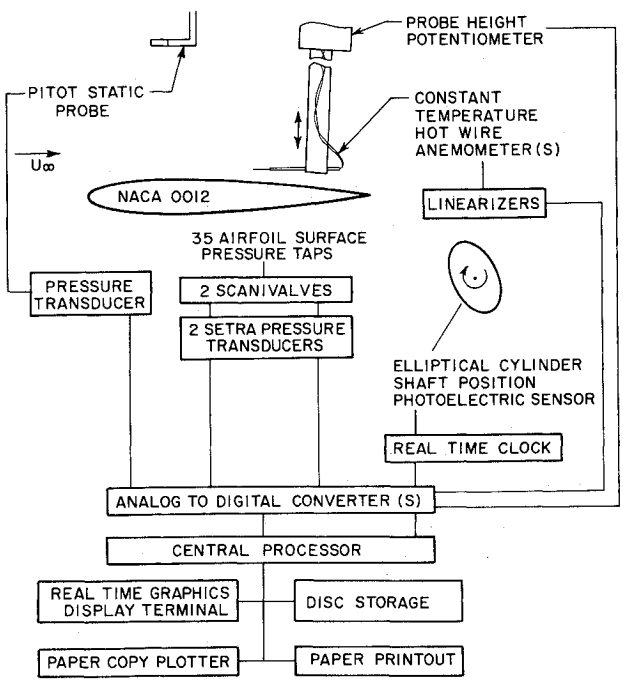

Fig. 1 Instrumentation block diagram.

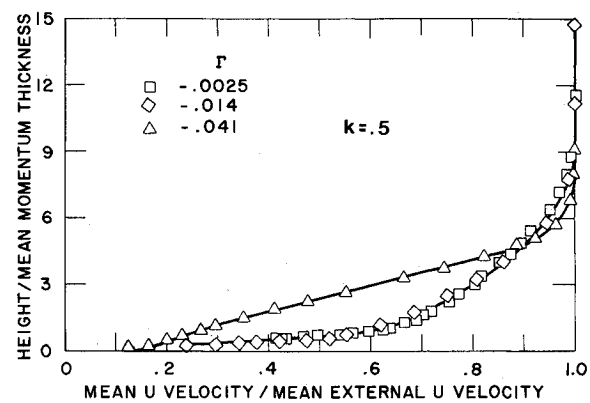

Fig. 2 Variation in mean velocity profiles due to mean pressure gradient at constant reduced frequency, $k = 0.5$.

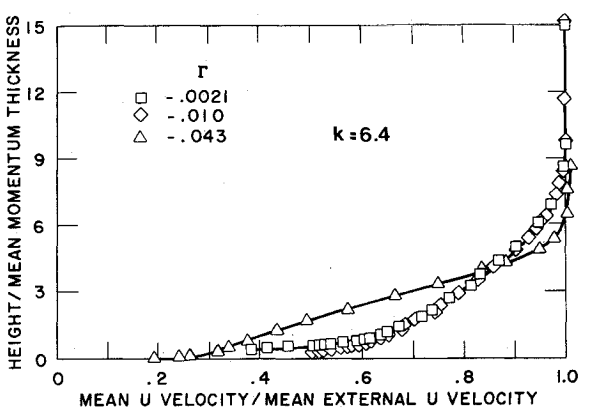

Fig. 3 Variation in mean velocity profiles due to mean pressure gradient at constant reduced frequency, $k = 6.4$.

airfoil. Measurements of the velocities induced by the elliptic cylinder in the plane of the airfoil chord (without the airfoil in the wind tunnel) show that the perturbation is dominated by an unsteady upwash concentrated near the airfoil trailing edge.[9,10] The upwash is primarily a constant phase or nonpropagating disturbance, with only a minor contribution to the airfoil pressure distribution being made by the propagating portion of the excitation. If the measured upwash (in the absence of the airfoil) is used as an input to Theodorsen's solution, the measured mean pressure difference distribution is accurately predicted. The unsteady part of the measured difference pressure distribution agrees well with the prediction for $k < 1$, while amplitudes are overpredicted for higher frequencies.[9]

Data given in Ref. 11 show that the zero pressure gradient flat-plate turbulent boundary layer in this tunnel and installation is consistent with accepted turbulent boundary layers. The unsteady pressure distribution is described in Refs. 9 and 10. The experimental conditions are given in Table 1.

Buri's form of the mean nondimensional pressure gradient,

$$\Gamma = \frac{\bar{\theta}}{U_e}\frac{dU_e}{dx}(Re_\theta)^{1/4}$$

is useful in defining test conditions. For our profiles. Γ was between -0.002 and -0.042, $\Gamma \sim -0.06$ corresponds to separation for a steady mean flow.[13] Γ may be written in steady flow as

$$\frac{\theta}{40C_f}\frac{1}{U_e}\frac{dU_e}{dx}$$

which is closely related to Clauser's alternate form

$$\beta = \frac{\delta^*}{\tau_w}\frac{dp}{dx}$$

The advantage of using Clauser's β or Buri's Γ to define the pressure gradient is that the boundary-layer history is implicitly included.‡

Boundary-layer velocities were measured using either a single hot wire (determining longitudinal velocity) or a cross wire (determining both longitudinal and normal velocities). The velocity probes were motor driven across the boundary layer, with the position being given by a linear potentiometer. Flow Corporation constant-temperature anemometers, linearizers, and sum difference amplifiers were used to produce the u and v velocities.

With the exception of some of the low-pressure gradient data, for which an analog system was used, the velocities and pressure were digitized, ensemble averaged, converted to nondimensional form, and plotted on-line (Fig. 1). This procedure allowed monitoring of the progress of the experiment and, in particular, indicated when additional cycles of data were needed in order to properly define the unsteady quantities. The required number of cycles depended on the signal-to-noise ratio of the periodic to fluctuating amplitudes and ranged from 100 to 4096.

For data taken with the single hot wire, only $\langle u\rangle = \bar{u}+\tilde{u}$ and $\overline{u'u'}$ were obtained, while data§ taken with the cross wire also included $\langle v\rangle$, $\langle u'u'\rangle$, $\langle v'v'\rangle$, and $\langle u'v'\rangle$, where u' is defined to have zero time average and ensemble average. These data have been stored on tape and provided to Dr. Carr at NASA Ames Research Center.[1]

Experimental Results

The experimental results are presented in terms of mean profiles for the velocities and Reynolds stresses, ensemble-averaged velocity profiles, and Fourier amplitudes and phase lag distributions for these quantities.

The estimated experimental uncertainties are as follows:

$u \simeq \pm 1\%\bar{U}_e$, $\tilde{u}$, $\tilde{v} \pm 3\%\tilde{u}_e$ if $\tilde{u}_e > 1\%$ of $\bar{u}_e$

$\pm 10\%\ \tilde{u}_e$ if $\tilde{u}_e < 1\%$ of $\tilde{u}_e$

$\overline{u'u'}$, $\overline{v'v'}$, $\overline{u'v'} \sim \pm 5\%$ of local value,

$\widetilde{u'u'}$, $\widetilde{v'v'}$, $\widetilde{u'v'} \sim \pm 10\%$ of local value

Phase to $\sim \pm 3$ deg

The graph of mean u velocity vs distance normalized by the mean momentum thickness is shown in Fig. 2 for the case where the elliptic cylinder was rotating at $k=0.5$. Three curves are plotted, corresponding to three local mean pressure gradients, $\Gamma = -0.0025$, -0.014, and -0.041. Data for the same geometric situation are replotted in Fig. 3 for $k=6.4$. The increasing pressure gradient makes the profile fuller near the wall and more concave near the outer edge of the boundary layer.

The mean velocity profiles at approximately the same local mean pressure gradient of $\Gamma \sim -0.014$, for four reduced frequencies $k=0.5$, 1.0, 2.0, and 6.4 are shown in Fig. 4. Except for the $k=6.4$ case for which Γ is slightly smaller, the differences between the profiles are no greater than the experimental error. The slight difference in Buri's pressure gradient parameter with reduced frequency is probably due to the increased mean circulation resulting from the higher cylinder rotation rate.

However, for the higher-pressure gradient case, $\Gamma = -0.030$, seen in Fig. 5, differences due to reduced frequency

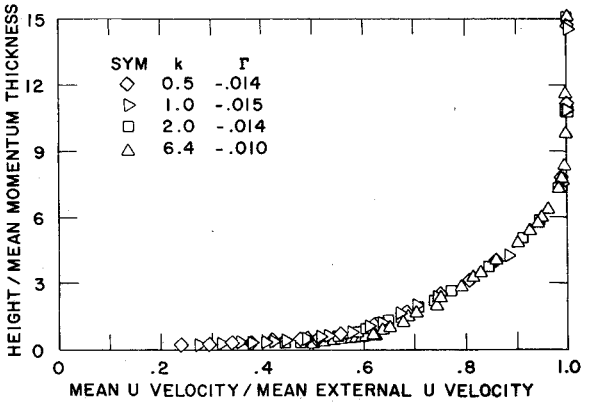

Fig. 4 Variation in mean velocity profiles due to reduced frequency at constant mean pressure gradient, $\Gamma = -0.014$.

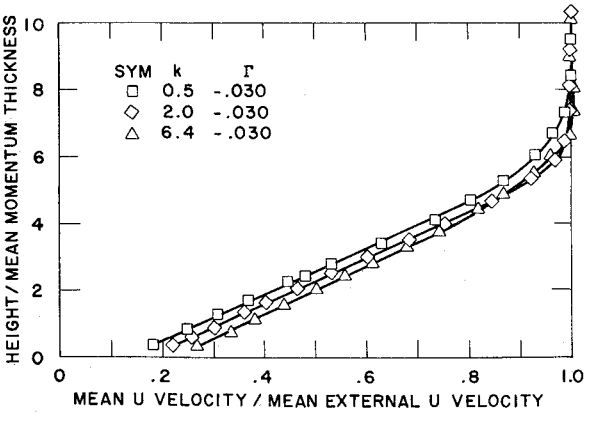

Fig. 5 Variation in mean velocity profiles due to reduced frequency at constant mean pressure gradient, $\Gamma = -0.030$.

‡That is, von Kármán's integral relation may be used to relate β or Γ to the flow at the boundary layer,

$$\beta = \frac{\delta^*}{\tau_w}\frac{dp}{dx} = \frac{H}{H+2}\left[\frac{U_e^2}{U_\tau^2}\frac{d\theta}{dx} - 1\right]$$

$$\Gamma = \frac{\theta}{80\tau_w}\frac{dp}{dx} = \frac{-1}{80(H+2)}\left[\frac{U_e^2}{U_\tau^2}\frac{d\theta}{dx} - 1\right]$$

Hence, either Clauser's β or Buri's Γ are measures of the departure of the turbulent boundary layer from the flat-plate equilibrium flow. If β or Γ are pure constants (i.e., independent of Reynolds number), then the flow in question is self-similar. In any case, β or Γ represent the ratio of two forces; one is the force per unit volume applied to the boundary layer from outside the boundary layer and the other is the force per unit volume applied by the wall through the shear stress, where the volume is normalized to either the displacement or momentum defect thickness. The presence of the products of boundary-layer parameters implies that the unsteady boundary layer offers the possibility for rectification and multiples of the frequency of excitation.

§Note the decomposition $u = \bar{u}+\tilde{u}+u'$ implies only that u' has a zero temporal mean. There is no intent to imply that u' is independent of frequency of excitation, i.e., in the notation of Ref. 14

$$u'(x,y,t) = u_0'(x,y,t) + u_1'(x,y,t,e^{i\omega t})$$

except that we normalize u_1' such that $u_1' \to 0$ as $\omega \to 0$.

are clear. Increased reduced frequency has a similar effect on the profiles as the reduced pressure gradient. The inflection of the profiles is reduced; thus the profile looks less like a separation profile.

Ensemble-averaged velocity profiles are plotted in Fig. 6 for mean pressure gradient $\Gamma = -0.014$ and reduced frequency 0.5. The profiles give the ensemble averaged velocity vs distance for several representative times in the rotational cycle. For this pressure gradient, all of the profiles are without inflection points at all times. The reduced unsteady amplitudes at high frequency are seen in Fig. 7 for $\Gamma = -0.010$ and $k = 6.4$. All profiles remain well behaved.

Figure 8, for $k = 0.5$ and $\Gamma = -0.041$, shows quite a different character, as the profile shape alternates between a large inflection and incipient separation and no inflection during the rotation cycle. Figure 9 illustrates the higher frequency $k = 6.4$ at $\Gamma = 0.043$. Note a moderately inflected profiles is maintained throughout the cycle, probably due to the smaller unsteady amplitudes.

The unsteady velocity data of Figs. 6-9 may also be reduced to distribution of Fourier amplitude and phase lag across the boundary layer. Figure 10 presents the amplitude of the fundamental harmonic, normalized by the amplitude of the same harmonic of the external flow, for the same cases as Fig. 4, $\Gamma \sim -0.014$, $k = 0.5$, 2.0, and 6.4. The high scatter seen for $k = 6.4$ is a result of an insufficient number of averages for the relatively small velocity amplitude present. The most striking feature of these plots is the large value of the unsteady amplitude overshoot, which ranges from 2.4 at $k = 0.5$ to 1.7 at $k = 6.4$. The height at which this maximum occurs decreases with increasing reduced frequency. Also shown in Fig. 10 is the unsteady amplitude profile from Ref. 7, measured on a flat plate in an adverse pressure gradient. As discussed below, this profile is at least qualitatively similar to the higher-frequency profiles presented here.

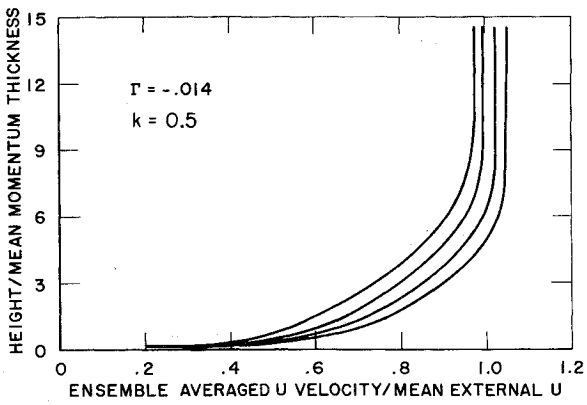

Fig. 6 Ensemble-averaged velocity profiles, $k = 0.5$, $\Gamma = -0.014$.

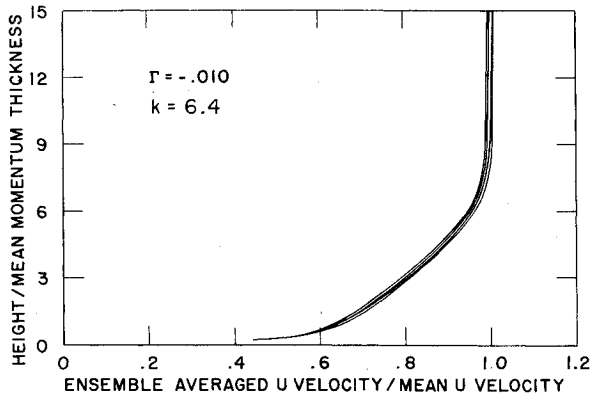

Fig. 7 Ensemble-averaged velocity profiles, $k = 6.4$, $\Gamma = -0.010$.

Figure 11 shows the same quantities at a higher-pressure gradient, $\Gamma = -0.030$. In addition, the vertical velocity amplitude $\tilde{v}$ is shown. As in the lower Γ case, the maximum $\tilde{u}$ amplitude overshoot is at $k = 0.5$, with lower values for $k = 1.0$, 2.0, and 6.4. However, the height of this maximum decreases less rapidly with increasing reduced frequency than in the data shown in Fig. 10. The $\tilde{v}$ amplitudes all drop monotonically to zero at the wall.

Comparing Figs. 10 and 11, the effect of pressure gradient is much more apparent for lower frequencies, as the maximum overshoot increases from 2.4 times the external amplitude to 5.6 times the external amplitude at $k = 0.5$, while remaining nearly constant for $k = 6.4$. The height of the maximum, at constant k, also increases for higher-pressure gradients.

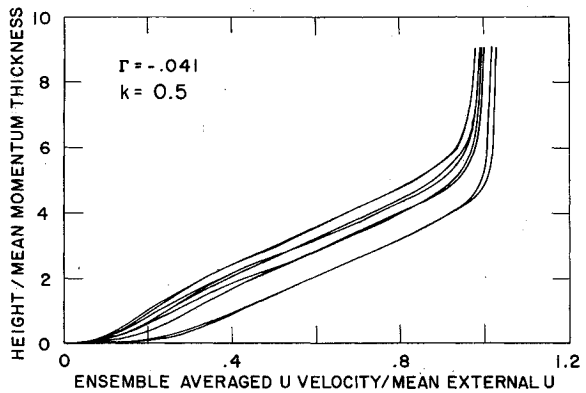

Fig. 8 Ensemble-averaged velocity profiles, $k = 0.5$, $\Gamma = -0.041$.

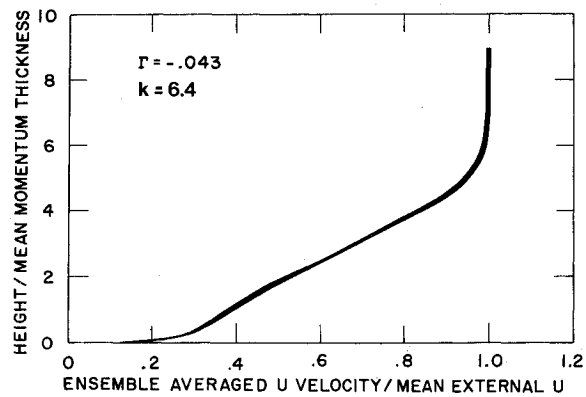

Fig. 9 Ensemble-averaged velocity profiles, $k = 6.4$, $\Gamma = -0.043$.

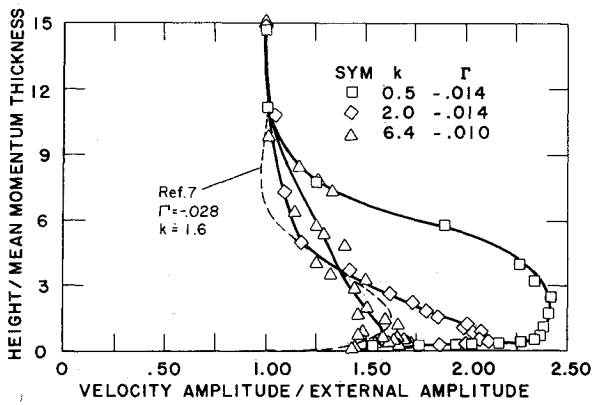

Fig. 10 Amplitude of fundamental harmonic u velocity; variation due to reduced frequency at fixed mean pressure gradient, $\Gamma = -0.014$.

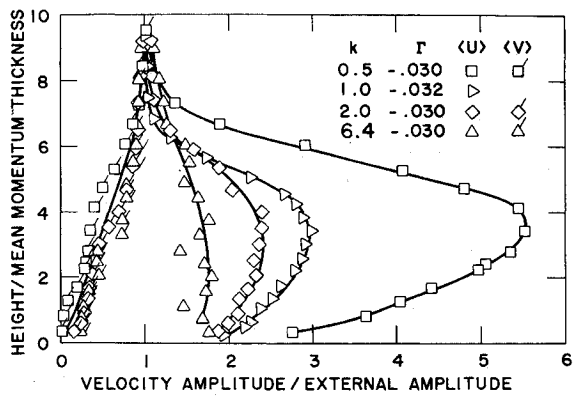

Fig. 11 Amplitude of fundamental harmonic u and v velocity; variation due to reduced frequency at fixed mean pressure gradient, $\Gamma = -0.30$.

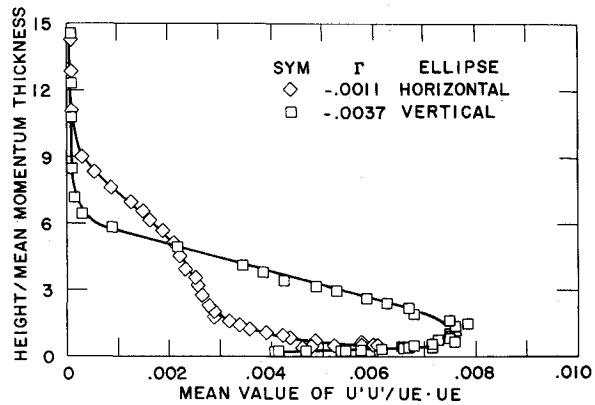

Fig. 12 Mean Reynolds stress, $\overline{u'u'}$ (steady elliptic cylinder and $\alpha = 0$ deg).

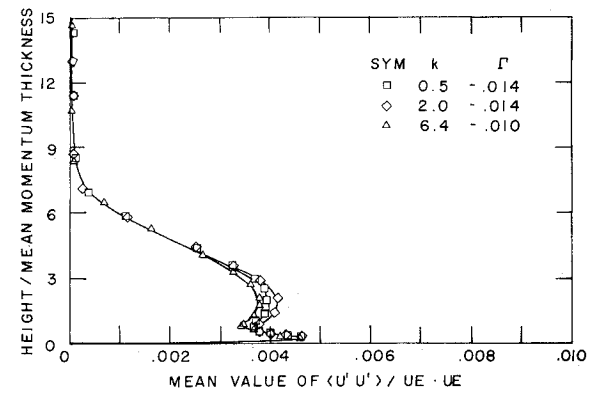

Fig. 13 Mean Reynolds stress, $\overline{u'u'}$ (rotating elliptic cylinder and $\alpha = 0$ deg).

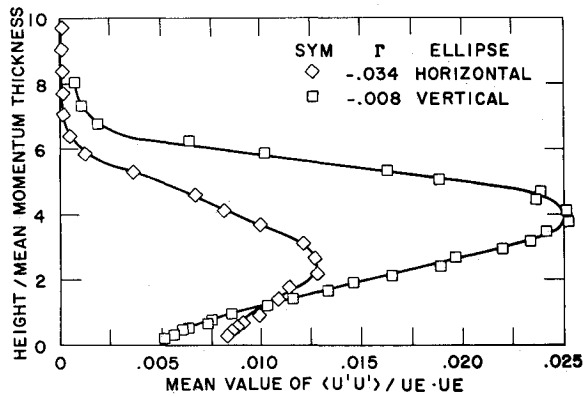

Fig. 14 Mean Reynolds stress, $\overline{u'u'}$ (steady elliptic cylinder and $\alpha = 10$ deg).

The next property of the velocity profiles to be illustrated are the mean Reynolds stresses, nondimensionalized by the square of the mean external velocity. Figure 12 shows $\overline{u'u'}$ for steady conditions at $\alpha = 0$. Note the large difference in profile shape between the high- and low-pressure gradient states. Increased pressure gradient increases and broadens the maximum $\overline{u'u'}$, removing the sharp peak near the wall. The time-averaged value of $\overline{u'u'}$ in the presence of the unsteady flow is shown in Fig. 13 for the same geometry. These profiles show the peak very close to the surface, as was observed in Patel's zero pressure gradient results[3] and in the low Γ steady data of Fig. 12.

Values of $\overline{u'u'}$ at the higher-pressure gradient steady case are shown in Fig. 14. The position of the maximum has moved further from the wall, and the maximum nondimensional amplitude has increased to 0.025 for the nearly separated case. Data taken with the cross hot wire, including measurements of $\overline{u'u'}$, $\overline{v'v'}$, and $\overline{u'v'}$, are shown in Fig. 15. For this higher-pressure gradient ($\Gamma = -0.30$) case, both $\overline{u'u'}$ and $\overline{v'v'}$ appear independent of k, while $\overline{u'v'}$ is smaller for $k = 0.5$ than for higher frequencies. The major effect of the increased pressure gradient is to remove the near wall peak in $\overline{u'u'}$ and to increase the maximum value by a factor of three, from 0.0052 to 0.015. This effect is similar to the effect of the pressure gradient on the unsteady amplitude discussed above.

Finally, the amplitude of the fundamental harmonic of $\langle u'u' \rangle$ for $\Gamma = -0.030$ and $k = 0.5$, 2.0, and 6.4 is shown in Fig. 16. Two peaks are seen, the larger somewhat above the position of maximum mean Reynolds stress $\overline{u'u'}$ and the second close to the wall. All amplitudes decrease sharply as frequency is increased: for example, the maximum of $\langle u'u' \rangle$ is 0.0085 at $k = 0.5$, but only 0.0003 at $k = 6.4$. Figure 17 shows amplitudes for the three quantities $\langle u'u' \rangle$, $\langle u'v' \rangle$,

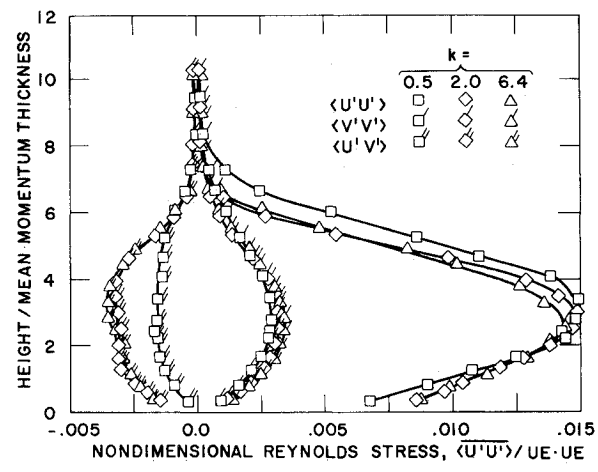

Fig. 15 Mean Reynolds stresses, $\overline{u'u'}$, $\overline{v'v'}$, and $\overline{u'v'}$ (rotating elliptic cylinder and $\Gamma = -0.030$).

and $\langle v'v' \rangle$ for $k = 0.5$, $\Gamma = -0.030$. The characteristic double maximum is seen in each curve; however, the height of the upper maximum differs.

Figure 18 presents profiles for the phase lag of the ensemble average of u and $u'u'$ for $k = 0.5$ and $\Gamma = -0.030$. The phase of $\langle u'u' \rangle$ is seen to differ by about 180 deg from that of $\langle u \rangle$ over the outer boundary layer, while the difference is less than 15 deg near the wall. The shift in phase of $\langle u'u' \rangle$ occurs at approximately 1.4 mean momentum thicknesses from the wall.

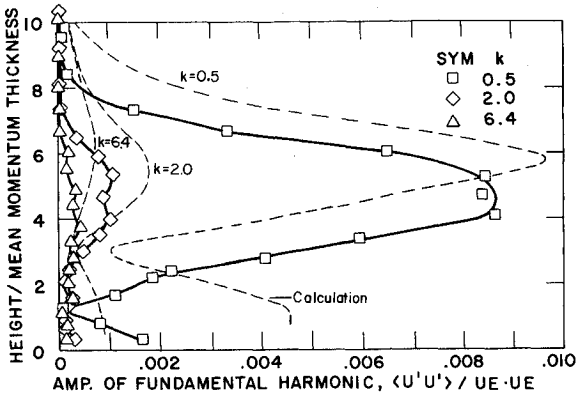

Fig. 16 Amplitude for the fundamental harmonic of the ensemble-averaged Reynolds stress, $\langle u'u' \rangle$ (variation with reduced frequency at $\Gamma = -0.030$).

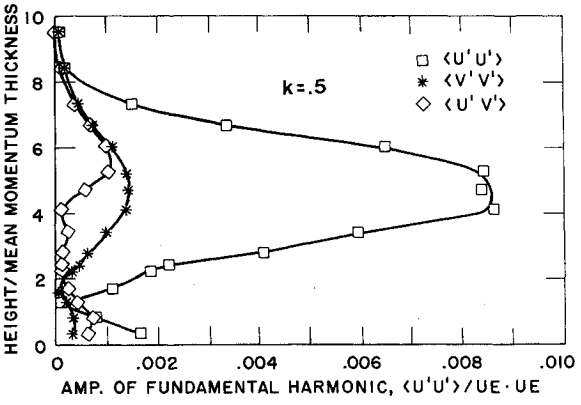

Fig. 17 Amplitude for the fundamental harmonic of the ensemble-averaged Reynolds stresses, $\langle u'u' \rangle$, $\langle v'v' \rangle$, $\langle u'v' \rangle$ ($k = 0.5$, $\Gamma = -0.030$).

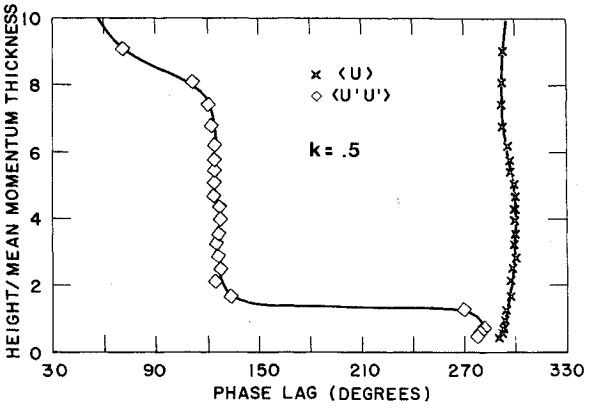

Fig. 18 Phase lags for the fundamental harmonic of $\langle u \rangle$ and $\langle u'u' \rangle$, $k = 0.5$ and $\Gamma = -0.030$.

Discussion

As mentioned previously, for high reduced frequencies, $k > 2.0$, the unsteady $\tilde{u}$ profile tends to become independent of pressure gradient and only weakly dependent on frequency. Figure 19 shows the ratio of the maximum unsteady amplitude to the external amplitude for all of the boundary layers presently studied, with $-0.002 < \Gamma < -0.043$. While large differences exist for $k < 2$, the value for higher k values approach a common value of approximately 1.8.

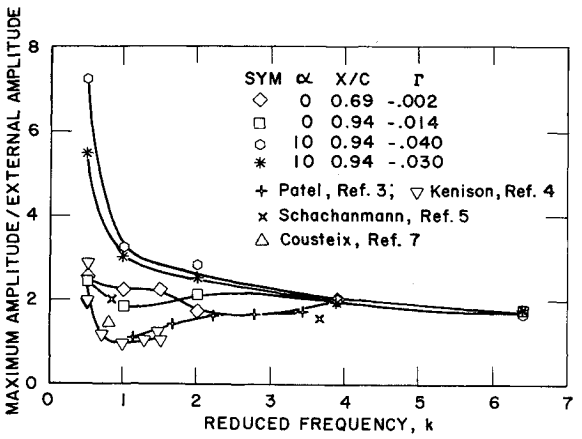

Fig. 19 Maximum overshoot of the fundamental harmonic of the $\langle u \rangle$ velocity plotted against reduced frequency (present and previous data are compared).

Figure 19 also shows results from previous high-frequency data. In computing a reduced frequency for flat-plate experiments, a length equal to one-half the distance from the leading edge or from the boundary-layer trip is used. These data, although generally of somewhat lower reduced frequency, do support the weak dependence of the unsteady profile on pressure gradient and frequency. This result parallels the theoretical predictions of Lighthill and of Lin for laminar boundary layers.[15,16]

As shown in Fig. 18 for a typical case, phase differences in $\tilde{u}$ across the boundary layer were generally small and in agreement with the results of Cousteix.[7] That is, over the outer part of the boundary-layer phase lags with respect to the outer flow of 10-20 deg were observed, with the position of maximum lag correspond to that of maximum amplitude. As the airfoil surface was approached the phase changed to a small lead (5-10 deg) over the external flow. Due to the relative sizes of the present hot-wire probe and boundary layer, data in the viscous sublayer could not be obtained.

The ensemble-averaged profiles were normally the only data recorded. However, for selected data points, up to 50 cycles of raw data were stored. One result of the analysis of these data was an estimate of the magnitude of the coupling terms $u'\tilde{u}$, $v'\tilde{u}$, and $v'\tilde{v}$. These terms are commonly neglected.[3] Based on the present data, the coupling terms were found to be at least one order of magnitude less than the equivalent turbulent terms, $u'u'$, $u'v'$, and $v'v'$. It is likely that if more cycles were analyzed for this purpose the ratio would decrease even further. From a theoretical viewpoint, such coupling terms should vanish if the ensemble average is taken at the same point in each cycle, as is true here.

An unsteady component of the ensemble-averaged Reynolds stress has been previously measured in boundary layers on flat plates in unsteady adverse pressure gradients. Cousteix et al.[7] show profiles of $\langle u'v' \rangle$ vs distance at several times in the oscillation cycle and then compare plots of $\langle u \rangle^2$ and $\langle u'v' \rangle$ against time at three fixed heights in the boundary layer. In agreement with the phase distributions shown in Fig. 18, $\langle u \rangle^2$ and $\langle u,v' \rangle$ were found to be "nearly in phase" near the wall and "roughly in phase opposition" in the outer boundary layer. Maximum amplitudes of $\langle u'v' \rangle$ varied with time from -0.002 to -0.0055, giving an approximation maximum Fourier amplitude of 0.0018, also similar to the present results (Fig. 17). Parikh et al.[17] also measured distributions of the amplitude of $\langle u'u' \rangle$ on a flat plate in an adverse pressure gradient. While no phase data were presented, plots of the amplitude vs distance exhibit the two key features of Fig. 16, a double peak and a reduction in amplitude with increased frequency.

For low frequencies and moderate amplitudes, a simple model of the unsteady boundary layer that accounts only for the change in thickness of the boundary layer over a cycle seems to be useful in providing a qualitative understanding of these results. In this model consider quantities, such as $\langle u\rangle(y,t)$ and $\langle u'u'\rangle(y,t)$, that to a first order are assumed to depend only on $y/\delta(t)$, where δ is a characteristic thickness, implying that

$$\frac{\partial\langle u\rangle}{\partial t} = \frac{-y}{\delta}\frac{\mathrm{d}\delta}{\mathrm{d}t}\frac{\partial\langle u\rangle}{\partial y}$$

Further, the data show a small-amplitude fundamental harmonic ($\tilde{u} \ll \bar{u}$ as well as $\partial\tilde{u}/\partial y \ll \partial\bar{u}/\partial y$) in the critical region. Hence the amplitude of $\langle u\rangle$ and $\langle u'u'\rangle$ are related by

$$\widetilde{u'u'}(y) = \tilde{u}(y)\left[\frac{\partial u'u'}{\partial y}\Big/\frac{\partial u}{\partial y}\right]\exp i(\phi_{u'u'} - \phi_u)$$

Note that this result is obtained for any reasonable choice of characteristic thickness δ.

This model states that $\langle u'u'\rangle$ will be in phase with $\langle u\rangle$ when the sign of $(\partial/\partial y)\,\overline{u'u'}$ is equal to that of $(\partial/\partial y)\,\bar{u}$, and 180 deg out of phase when they are not. For $k=0.5$ and $\Gamma = -0.030$ this leads to a calculation of a phase shift at $y/\theta = 3.0$ as compared with the measured location of $y/\theta = 1.4$. Predictions of the amplitude of $\widetilde{u'u'}$ made with this model agree only qualitatively with the measured amplitudes, as shown in Fig. 16. However in light of the simplicity of the model and since the profiles are not always similar with time (see Figs. 6-9), other factors are needed to provide a quantitative agreement with the data.

Conclusions

A series of experiments have been performed to determine characteristics of the turbulent boundary layer of a NACA 0012 two-dimensional airfoil subject to an oscillating external flow. Ensemble-averaged velocities and Reynolds stresses were measured over a wide range of reduced frequencies from nearly quasisteady to significantly greater than a reduced frequency of unity and of mean pressure gradients from a mildly adverse gradient to one producing incipient separation.

Mean profiles were found to be independent of reduced frequency for moderate adverse pressure gradients, but for steeper adverse pressure gradients, the mean profile was less like a separation profile as the frequency was increased.

Periodic velocity profiles had large increases in amplitude in the boundary layer as compared to external flow, but small phase differences from that flow. For low frequencies, the profiles were highly dependent on the mean pressure gradient, while the high-frequency profiles appeared to approach a universal profile independent of both frequency and pressure gradient.

Mean Reynolds stresses had a much stronger dependence on the mean pressure gradient than on reduced frequency, with both high- and low-pressure gradient data being smaller to previous results for roughly similar conditions. However, a periodic part of the Reynolds stress was measured and seems to be important. It was found to depend on the amplitude of the periodic velocities and on the normal gradients of the mean velocity and the mean Reynolds stress.

Correlation between the periodic and nonperiodic velocity components $(\overline{u'\tilde{u}})$ were found to be at least an order of magnitude smaller than the mean nonperiodic values $(\overline{u'u'})$. Theoretically, this value should be zero. The common neglect of these quantities appears to be justified.

Acknowledgment

This work was sponsored under Grant 80-0282 with the U.S. Air Force Office of Scientific Research, Dr. Michael S. Francis, Program Manager.

References

[1] Carr, L. W., "A Compilation of Unsteady Turbulent Boundary Layer Experimental Data," AGARD AG-265, Nov. 1981.

[2] Karlsson, S.F.K., "An Unsteady Turbulent Boundary Layer," *Journal of Fluid Mechanics*, Vol. 5, May 1959, p. 622.

[3] Patel, M. H., "On Turbulent Boundary Layers in Oscillatory Flows," *Proceedings of the Royal Society of London*, Ser. A, Vol. 353, 1977, pp. 121-144.

[4] Kenison, R. C., "An Experimental Study of the Effect of Oscillating Flow on the Separation Region in a Turbulent Boundary Layer," AGARD CP-227, Feb. 1978, Paper 20.

[5] Schachenmann, A. A. and Rockwell, D. O., "Oscillating Turbulent Flow in a Concial Diffuser," *Journal of Fluids Engineering, Transactions of ASME*, Vol. 98, Ser. 1, Dec. 1976, pp. 695-701.

[6] Simpson, R. L., Shivaprasad, B. G., and Chew, Y. T., "Some Important Features of Unsteady Separating Turbulent Boundary Layers," Paper presented at IUTAM Symposium on Unsteady Turbulent Shear Flows, Toulouse, France, May 5-8, 1981.

[7] Couteix, J., Houdeville, R., and Raynaud, M., "Oscillating Turbulent Boundary Layer with Strong Mean Pressure Gradient," Paper presented at 2nd Symposium of Turbulent Shear Flows, Imperial College, London, 1979, (also ONERA TP 1979-80).

[8] Telionis, D. P., "Review Unsteady Boundary Layers, Separated and Attached," *Journal of Fluids Engineering*, Vol. 101, March 1979, p. 29.

[9] Lorber, P. F. and Covert, E. E., "Unsteady Airfoil Pressures Produced by Periodic Aerodynamic Interference," *AIAA Journal*, Vol. 20, Sept. 1982, pp. 1153-1159.

[10] Lorber, P. F., "Unsteady Airfoil Pressures Produced by Perturbation of the Trailing Edge Flow," SM Thesis, Massachusetts Institute of Technology, Cambridge, Mass., Feb. 1981.

[11] Kanevsky, A. R., "Comparison of Pressure Distribution for Circulation Generated by Angle of Attack with that Generated by Trailing Edge Perturbation," SM Thesis, Massachusetts Institute of Technology, Cambridge, Mass., Feb. 1978.

[12] Clauser, F. H., "Turbulent Boundary Layers in Adverse Pressure Gradients," *Journal of the Aeronautical Sciences*, Vol. 21, Feb. 1954, pp. 91-108.

[13] Schlichting, H., *Boundary Layer Theory*, Vol. 6, McGraw-Hill Book Co., New York, 1968, p. 629.

[14] Romaniuk, M. S. and Telionis, D. P., "Turbulence Models for Oscillating Boundary Layers," AIAA Paper 79-0069, 1979.

[15] Lighthill, M. J., "The Response of Laminar Skin Friction and Heat Transfer to Fluctuations in the Stream Velocity," *Proceedings of the Royal Society of London*, Ser. A, Vol. 229, 1954, pp. 1-23.

[16] Lin, C. C., "Motion in the Boundary Layer with a Rapidly Oscillating External Flow," *Proceedings of 9th International Congress on Applied Mechanics*, Universite' de Bruxelles, Brussels, Vol. 4, 1956, pp. 155-167.

[17] Parikh, P. G., Reynolds, W. C., and Jayaraman, R., "Behavior of an Unsteady Turbulent Boundary Layer," *AIAA Journal*, Vol. 20, June 1982, pp. 769-775.